Methodology for determining aerosol optical depth from Brewer 300–320-nm ozone measurements

Franco Marenco, Alcide di Sarra, and John De Luisi

With a Brewer spectrophotometer, an estimation of total ozone is made from relative measurements of direct-sun ultraviolet radiation at six wavelengths from 300 to 320 nm. During normal operations, one of six neutral-density filters is selected automatically to maintain the detector in its linear response range. On the basis of these standard direct-sun observations, estimates of aerosol optical depth can be derived, provided that a calibration of the relative measurements is available for each neutral-density filter. To obtain the calibration, we implemented a routine to measure direct-sun signals with a fixed neutral-density filter and applied the Langley method to the measured photon counts. Results show that if a sufficiently large number of cloud-free mornings or afternoons is available, a reliable calibration can be achieved even at sea-level sites that are characterized by large aerosol variability. The derived aerosol optical depths appear consistent with those measured independently by a multifilter rotating shadow-band radiometer. Existing relatively long-term series of direct-sun ozone measurements by Brewer instruments may be used for retrieval of aerosol optical depth. © 2002 Optical Society of America

OCIS codes: 010.1110, 280.0280.

1. Introduction

Aerosols are solid and liquid particles suspended in the atmosphere, and their radiative effects are one of the major unknowns of the Earth's climate system.[1] Large uncertainties exist in the microphysical characterization of aerosols and in their global distribution.[2] The particles differ in composition and are mainly grouped into the following classes: sea salt, mineral dust, sulfates, carbonaceous aerosols (including black carbon), and mixed aerosols. The particle sizes range over several orders of magnitude (typically 10^{-2} to 10^2 μm); the shapes too can be widely different: spheres are usually assumed for liquid aerosols and irregular shapes or crystals for solid particles. Aerosols may also be classified as hygroscopic or nonhygroscopic particles; in the first case the size distribution is modified by humidity. Moreover, hygroscopic aerosols act as cloud condensation nuclei (CCN) and thus can influence cloud formation.

Deposition of aerosol particles can take place in either of two ways: Dry deposition is due to gravity, and wet deposition is due to washout by rain. For these two processes, aerosol residence times are estimated to be 1 to 10 days,[2–5] and accordingly the particles may be found to travel as much as ~5000 km from the source. This atmospheric lifetime is short compared, for instance, with the lifetimes of gaseous constituents such as CO_2, CH_4, and CFCs, which are decades to centuries: For this reason the aerosol content of the atmosphere is determined mainly by source neighborhood and atmospheric circulation. The global and regional distribution of the particles is both highly variable in time and nonuniform in space.[5,6]

Aerosols influence the climate directly through scattering and absorption of the incoming solar radiation: The scattering process determines a larger terrestrial albedo and thus a negative radiative forcing (see, e.g., Ref. 7); the absorption process, instead, is thought to cause heating of the Earth and more specifically of the atmospheric layers where the aerosols reside, thus possibly influencing a modification of the circulation patterns.[5] The net direct effect of aerosols on climate can result in a negative or a positive radiative forcing of a magnitude of 20 W/m^2 or more locally, which is comparable with the effect of clouds.[2]

Acting as CCN, aerosols can also produce an indi-

F. Marenco (franco.marenco@casaccia.enea.it) and A. di Sarra are with Ente per le Nuove Tecnologie, l'Energia e l'Ambiente, Italy. J. De Luisi is with the National Oceanic and Atmospheric Administration, Boulder, Colorado 80303.

rect climate effect. An increase of CCN concentration will increase the number of cloud droplets and decrease droplet size for a given liquid-water content, producing an increase of cloud albedo and lifetime: These effects are also thought to produce a negative radiative forcing.[6,8,9] It has been acknowledged as well that the net radiative effect of the hydrological cycle's modification by aerosols acting as CCN has not been quantified.[6] Also, the presence of absorbing CCN in cloud droplets may enhance absorption by as much as ~3 orders of magnitude with respect to that of pure water.[4]

The net effect of aerosols on climate is understandably difficult to quantify. It has been argued that negative climate forcing by anthropogenic aerosols owing to increased scattering and indirect cloud effects is comparable in magnitude (and opposite in sign) to climate forcing that results from an increased concentration of greenhouse gases (see, e.g., Ref. 1). Consequently, aerosols could be negating a significant part of the greenhouse effect: It has been suggested that aerosols are masking the real response of the climate system and that the temperature sensitivity of the Earth is higher than observed.[9]

In particular, desert aerosols are composed of mineral dust and thus undergo absorption of light with a single-scattering albedo range of 0.6 to 0.9.[5] Their effect on visible radiation is a major uncertainty but is believed to be of the order of $+20$ to $+40$ W/m^2 over arid regions and of -5 to -15 W/m^2 over oceans[2]; the radiative effect of the dust might be significant in the infrared range as well. The Sahara desert is one of the well-known major sources of mineral dust that travels thousands of kilometers worldwide. The contribution of Saharan dust to the total aerosol burden of the atmosphere is estimated to be 60–200 million tons per year.[3] Mineral aerosols are also important in the Mediterranean environment, as they represent one of the major sources of nutrients for phytoplankton and other aquatic organisms.[10,11] These aerosols are a consequence of soil erosion by atmospheric activity. It is estimated that ~30% of the total atmospheric mineral dust load can be ascribed to human activities through the processes of desertification and land misuse.[2] Saharan dust lifted by strong convective motions owing to surface heating in the desert has been observed at altitudes of ~5 km (see, e.g., Ref. 3) and in some cases as high as ~8 km.[12] The dust can then be transported over very long ranges.[3]

Better quantification of the global net effect of aerosols on the Earth's climate requires long-term worldwide monitoring of the aerosol content, ideally measured by comparable methods. Local aerosol observations have been performed sporadically over the past four decades, but they inadequately portray the global distribution of aerosols. Satellite measurements have the advantage of being global, but they heavily rely on assumptions concerning the particle properties (single scattering albedo, index of refraction, particle shape, etc.) and the underlying surface albedo.[5] Local observations are commonly performed by optical remote sensing or *in situ* instrumentation. Remote sensing from the ground with sunphotometers yields the column-integrated optical depth; vertical profiles can be obtained by lidar. Remote sensing data from different instruments (from both satellite- and ground-based stations) usually cannot be compared precisely because they address different wavelengths. Also, satellites view a large region, whereas local measurements represent points on the globe.

A major issue that needs to be resolved concerns the magnitude of the natural and anthropogenic components of the global aerosol population. The importance of improving knowledge of these issues was the motivating factor for establishing an aerosol observing station at the island of Lampedusa, Italy (35.5 °N 12.6 °E), within the facilities of the Station for Climate Observations of the National Agency for New Technology, Energy and Environment of Italy. Lampedusa is a small rocky island, relatively isolated, in the southern Mediterranean Sea, approximately 100 km east of Tunisia and 200 km north of Lybia. Because of the proximity of the island to the African continent, the Sahara desert is assumed to be the major source of aerosols there.

In this paper we present a simple methodology for estimating the aerosol optical depth from a Brewer spectrophotometer by use of a data set of total-ozone measurements (the ds routine; see Ref. 14). The Brewer instrument operates in the UVA–UVB spectral range and can be programmed to measure the following quantities: spectral global irradiance, spectral direct radiance, and total ozone. Its description can be found in Ref. 14. We use the double-monochromator version of the Brewer spectrophotometer, and the spectral range is 285–366 nm at intervals of 0.5 nm with a resolution of 0.6 nm. Global irradiance is absolutely calibrated with a 1000-W standard source of spectral irradiance, traceable to a standard from the U.S. National Institute of Standards and Technology. The instrument's stability is regularly monitored with a 50-W lamp. Our instrument (Brewer MK-III #123) has not been calibrated for absolute direct radiance observations, nor does it need to be for the research reported here.

Total-ozone measurements are normally available at all Brewer stations: Therefore the method introduced here may also be used to retrieve the aerosol optical depth from previous observational records or when spectral direct-sun scans have not been specifically scheduled. Thus, using total-ozone measurements instead of direct-sun spectral scans to infer aerosol optical depth permits the retrieval of aerosol information also when aerosol measurements have not been expressly implemented. Thus there is an opportunity to use virtually all the data derived from the Brewer network, i.e., from ~100 stations throughout the world, among which the oldest have been operating for more than 15 years.

Table 1. Ozone Absorption Coefficients (k_{O_3}) and Filter 3 Calibration Constants (I_0) at the Brewer Wavelengths[a]

Wavelength (nm)	k_{O_3} (cm^{-1})	I_0 for Filter 3 (photon counts $\times 10^7$)
303.2	2.6222	2.482 ± 0.068
306.3	1.8326	2.376 ± 0.048
310.1	1.0003	2.025 ± 0.041
313.5	0.7198	3.517 ± 0.070
316.8	0.3910	3.769 ± 0.074
320.1	0.3127	4.114 ± 0.081

[a]The ozone absorption coefficients are taken from Molina and Molina.[13] The calibration constants refer to Brewer spectrophotometer # 123.

2. Mathematical Representation of Direct-Sun Aerosol Optical Depth Measurements

The Brewer spectrophotometer performs ozone measurements each time the ds command is issued. The instrument is oriented toward the Sun, and a series of five direct-sun observations at six wavelengths is performed (the wavelengths are listed in Table 1). The 303.2-nm wavelength is used for wavelength calibration purposes, and the ratios among the other five wavelengths are used to compute total ozone value, expressed in Dobson units.[14] The methodology presented here uses these photon-count data, along with the ozone value, to infer the aerosol optical depth.

The first step consists in correction of instrumental dead time and subtraction of dark counts. Then one can use Beer's law to determine the atmospheric total optical depth:

$$\tau_{tot} = \frac{1}{m} \ln\left(s\, \frac{I_0}{I} \right), \tag{1}$$

where I and I_0 are, respectively, the direct-sun radiance measured by the Brewer spectrophotometer at ground level and the extraterrestrial radiance at the same wavelength. The factor s is a correction factor that accounts for the seasonal correction for the Sun–Earth distance and is estimated for Julian day j with the following approximate formula[15]:

$$s = 1 + 0.033 \, \cos\left(\frac{2\pi j}{365.25} \right). \tag{2}$$

Air-mass factor m is a geometrical coefficient that takes into account the direct beam slant path through the atmosphere, where τ_{tot} is the optical depth for a vertical path ($m = 1$ for a vertical path; otherwise $m > 1$). For a plane-parallel atmosphere, $m = 1/\cos\theta$, where θ is the solar zenith angle; however, owing to the curvature of the Earth, the optical path is actually longer. For $\theta < 60°$ the inverse cosine law can be safely used; for larger angles the exact computation of the air-mass factor can be performed with the method described in Ref. 16, and it depends on the vertical distribution of the atmospheric attenuator that is being considered.

The aerosol optical depth can then be deduced by subtraction of the known contributions of other spe-cies to τ_{tot}. In the wavelength range of the Brewer measurements, these are Rayleigh scattering and ozone; SO_2 might be considered as well, but it has been neglected in the present study. Therefore

$$\tau_{aer} = \tau_{tot} - \tau_{ray} - \tau_{O_3}$$

$$= \tau_{tot} - \frac{p}{p_0} \tau_R(\lambda)$$

$$- D_{O_3} k_{O_3}(\lambda) \frac{\ln 10}{1000}, \tag{3}$$

where p is the atmospheric pressure at the measuring site, $p_0 = 1013.25$ hPa is the standard atmospheric pressure, D_{O_3} is the ozone column in Dobson units, $k_{O_3}(\lambda)$ is the ozone absorption coefficient expressed in inverse centimeters (see Table 1; we used the values given in Ref. 13), and $\tau_R(\lambda)$ is the Rayleigh scattering optical depth from sea level to infinity under standard atmospheric conditions.[17,18]

As a matter of fact, inasmuch as the air-mass factor depends on the vertical profile of each atmospheric attenuator, a more general form for Eq. (3), which takes into account the factors for Rayleigh, ozone, and aerosol contributions, is

$$m_{aer}\tau_{aer} = m\tau_{tot} - m_{ray}\tau_{ray} - m_{O_3}\tau_{O_3}. \tag{4}$$

Equation (4) requires that m_{ray}, m_{O_3}, and m_{aer} be evaluated separately and thus that at large values of m the vertical distributions of the three species must be known. These distributions differ substantially from one another, because the density profile of the uniformly mixed gas decreases exponentially from the surface with a scale height of ~8 km; the ozone distribution is peaked in the lower stratosphere near 22 km; and aerosols are concentrated mostly in the boundary layer.

3. Calibration

In a previous paper,[19] a simple methodology was described with which aerosol optical depth can be inferred by use of the data of the direct-sun spectral radiance (ss routine) obtained from the University of Thessaloniki instrument (Brewer spectrophotometer # 086). That method assumed calibrated direct-sun radiances, and the instrument had been calibrated for absolute direct-sun responsivity.[20,21] Because absolute calibration is difficult to achieve for direct-sun measurements, spectral scans of direct-sun irradiance are rarely performed at most stations.

The method described here can be applied to an uncalibrated instrument because the reference calibration is performed with the Langley method. Moreover, the method uses the signal of the total-ozone direct-sun measurements (ds routine) that is implemented at all Brewer stations.

Using Eq. (1) requires that the measurements of direct-sun radiance I be absolutely calibrated, and an independent data set containing the spectral solar extraterrestrial irradiance I_0 is needed. Absolute calibration of direct-sun measurements obtained
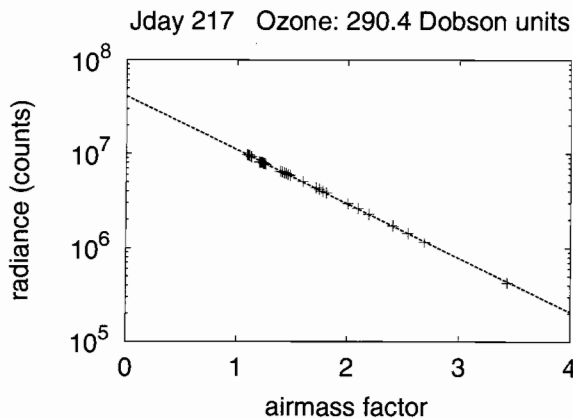
Fig. 1. Example of a Langley plot: the measured direct-sun radiance I at 320.1 nm for the morning of 4 August 2000, expressed in photon counts, is displayed versus the air-mass factor. The data were taken with neutral-density filter 3. Dashed line, a linear regression. Extraterrestrial irradiance I_0 can be obtained by extrapolation of I to $m = 0$: for this plot the result is $I_0 = (4.122 \pm 0.034) \times 10^7$ photon counts.

from a Brewer spectrophotometer can be achieved by calibrated measurements of the global and diffuse components.[21] Absolute calibration of the instrument can also be obtained by comparison of measured intensities to the values of a known source, such as a standard lamp or the Sun.

It is definitely simpler to conduct the experiment if the Sun itself is used for calibration: The atmospheric attenuation must be removed, and this is possible by Langley extrapolation to a zero air-mass factor[16,22,23] (see also Ref. 24 for application to the Brewer spectrophotometer). Because, in Eq. (1), only the ratio between I_0 and I is required, a known extraterrestrial spectrum is not needed: I_0 expressed in instrumental units (photon counts in our case) *is* the calibration constant if optical depth only is to be measured. If researchers actually need a radiance calibration, it might be obtained by scaling of this constant according to an independent measurement of the extraterrestrial spectrum (but, if this operation is performed, care is needed to take into account the effect of the slit function of the Brewer instrument).

One obtains the Langley extrapolation by examining the variation of the measured ground-level radiance as the air-mass factor varies during half a day. On the assumption of a constant optical depth τ_{tot}, we expect from Eq. (1) that the plot of I versus m on a logarithmic scale will be a straight line, as in Fig. 1. The y intercept of this line represents the intensity for $m = 0$ (no atmosphere), and thus sI_0. To simplify our analysis we set $m_{ray} \simeq m_{aer} \simeq m_{O_3} \simeq m$; this simplification is acceptable if large values of air-mass factor are not included: In the data that we present, therefore, it is always $m \leq 4.5$. Thomason *et al.*[16] have shown that this simplification introduces a systematic error in I_0 that in extreme cases is less than 2%.

A note on how the Brewer spectrophotometer op-

erates during ds operation is needed. As has been said, this type of measurement was designed to derive ozone and not radiance: Therefore the absolute level of intensity is usually not needed, and only ratios of signals at different wavelengths are normally required; see, e.g., the retrieval scheme described in Refs. 25 and 26. To keep within the optimal working range of the photomultiplier, before every measurement the instrument's software automatically selects a neutral-density filter, based on signal intensity. The filters are numbered 0 through 5 (0 is the number for no filter). Therefore a different calibration constant for each filter and for each wavelength exists, and there are $6 \times 6 = 36$ different constants.

Ideally, a separate Langley plot should be made for each filter. However, in this case only a few points would be available for each of the filters. To bypass the automatic selection of the filter we modified the software driving the Brewer spectrophotometer; this provides a means to force the instrument to use the filter that we choose. During the summer at Lampedusa the automatic filter-selection algorithm most of the time selects filters 0–3; filter 4 is seldom used. We chose 3 as our reference filter because this filter's transmission is sufficiently low that the detectors are protected and operated in their linearity range. The drawback is that, with low signals (large solar zenith angle), relative errors are larger than with a less-attenuating filter.

The calibration proceeds in two steps. First, a calibration with the Langley extrapolation method is performed with filter 3. Then the interfilter calibration is derived.

A. Calibration with the Langley Method

The calibration campaign was conducted in the summer of 2000, during a 10-week period extending from 28 June to 6 September 2000. This period was selected for two reasons: first, the small value of m (close to 1) that is reached at noon during summer at this latitude permits a larger interval for Langley extrapolation and second, the probability of having cloud-free conditions is high in this season. The Brewer spectrophotometer was scheduled to make several ds and d3 measurements: The latter refers to the modified Brewer routine that bypasses filter selection and uses filter 3 every time. The former is the regular measurement with the automatic filter selection included. Thus, direct-sun measurements with all filters were alternated with measurements for which filter 3 was used.

Langley extrapolation can be performed by extracting filter 3 data from the data set. Because the main assumption is that optical depth is constant during an entire morning or afternoon, a major requirement is that the Sun not be masked by clouds: The selection of cloud-free periods is based on visual observations of the sky. All Langley plots in the data set are also checked individually to verify that the data align well on a straight line: Large deviations over relatively short times may suggest the presence of clouds that were missed in the visual observations; small
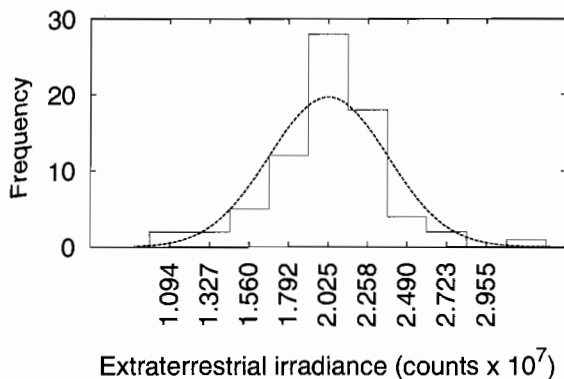
Jdays 180-249 / 2000

Fig. 2. Values of the calibration constant for the channel at 310.1 nm and filter 3 found for the 74 half-days of the calibration period. The average value is $I_0 = 2.025 \times 10^7$ photon counts, and the standard deviation of the data is $\sigma = 0.349 \times 10^7$ counts. A Gaussian distribution with these parameters is shown as a dashed curve. The standard deviation of the mean is obtained as $\sigma/\sqrt{74} = 0.041 \times 10^7$ counts, where 74 is the number of independent measurements.

and slower trends, instead, are more characteristic of variations in the aerosol load. All data that do not comply with the criteria described above are rejected. Based on this approach, we retained a set of 74 valid plots from 140 half-days. However, it has to be said that there is no guarantee that the data actually contain no optical depth variation (indeed, we show later in this paper that there is one). In fact, slow and monotonic aerosol optical depth variations may produce well-aligned data that may be confused with correct Langley plots. Also, subvisual cirri with very low optical depth ($\tau < 0.03$) may produce small nonlinearities.

An example of a Langley plot is displayed in Fig. 1: For each of such plots we obtain a value of I_0. The results show a significant day-to-day variability of the value of I_0, which we ascribe to the above-mentioned interferences with the Langley extrapolation method. Usually, calibration with Langley plots is performed at high altitude to minimize the influence of aerosols and their variations. In our case, instead, we used simple statistics to infer the correct calibration constant and to reduce random errors.

Figure 2 shows the distribution of the derived values of I_0 at 310.1 nm, determined from the 74 selected Langley plots. Nine intervals are chosen, with the central values indicated on the x-axis scale (the width of each interval is $6\sigma/9$, where σ is the standard deviation of the data set). The data are randomly distributed about their average, confirming that the deviation from the mean can be attributed to random errors. Similar results were obtained at the other wavelengths.

It is assumed that the atmospheric disturbances that might be present when Langley plots are produced at sea level act as the random process that produces these discrepancies. Thus we may take

the mean as representative of the calibration constant. The standard deviation *of the mean* is assumed to be the calibration error. The calibration constants for the six wavelengths are listed in Table 1. The uncertainty in I_0 that results from this data set, ~2%, may lead to an uncertainty of $\Delta\tau_{aer} \leq 0.02$ in the aerosol optical depth (this absolute error decreases when the solar zenith angle increases). This uncertainty is of the same order of magnitude as the error that is due to photon-count statistics ($\Delta\tau_{aer} \sim 0.01-0.07$, depending on signal intensity and solar zenith angle).

Our statistical error of 2% in I_0 must be compared with the uncertainty produced with other calibration methods. Bais,[21] for instance, introduced a calibration method for the direct-sun Brewer radiance obtained with quasi-simultaneous measurements of the direct, diffuse, and global components of the radiation field, using a shading disk to exclude the direct component in the diffuse irradiance measurements. This method, however, relies on the calibration accuracy of the global and diffuse irradiance (~2%) obtained with a standard lamp. Moreover, the result is affected by the cosine response of the instrument, which must be accurately known, and by the change in shape of the disk shadow with solar zenith angle. The overall error in I_0 that resulted from this procedure was thus found to be ~4%. Another way to determine the extraterrestrial solar radiance that is currently being investigated is to perform a radiometric calibration of the direct component directly with a standard lamp.[27] However, it is difficult to establish a reliable methodology, and the resultant indeterminacy is difficult to estimate. It is our opinion that, even when the uncertainties in the lamp emissivity, distance, and deviation from an ideal point source are taken into account, a final calibration error smaller than 2% is unlikely to be achieved.

B. Interfilter Calibration

So far we have obtained I_0 at the six wavelengths for measurements performed with filter 3. The next step consists in deriving the calibrations for the other filters, which we do by determining the ratio of the transmissivity of the other filters to the transmissivity of filter 3. Three subsequent direct-sun measurements are performed closely in time. The first measurement uses filter 3, the second uses a different filter, and the third uses 3 again. The three measurements are taken within 15 min because each ds routine takes approximately 4–5 min. As for a Langley calibration, only data for clear-sky days have been used.

For each wavelength the intensity of filter 3 is interpolated to the time at which the measurement with another filter was made. Interpolation is done with the air-mass factor used as the independent variable, allowing us to apply the Beer's law simple relationship [Eq. (1)], by assuming a constant τ_{tot} within the 15-min period considered.

This procedure was repeated several times, distributed over the clear-sky days of the 10-week calibra-

Filter Number	Number of Observations	Calibration Ratio Relative to Filter 3	Transmissivity	Neutral Density	Nominal Neutral Density
0	23	36.41 ± 0.46	1.0000	0.00	0.0
1	37	13.983 ± 0.048	0.3841	0.42	0.5
2	113	4.759 ± 0.015	0.1307	0.88	1.0
3	945	1.000 ± 0.000	0.0275	1.56	1.5
4	–	[b]	[b]	[b]	2.0
5	–	[b]	[b]	[b]	2.5

[a]Determined with the method described in the text for Brewer spectrophotometer # 123.   Filter transmissivities and neutral densities are also shown and are compared with nominal neutral densities.
[b]Not available.

tion period.   The calibration ratios listed in Table 2 were derived.   We made control measurements by applying this method to autocalibrate filter 3 with itself; as expected, a value of 1 was obtained.   Deviations as large as 20% are rarely found in single values (with the filter 3 autocalibration as well); the calibration ratios and the errors given in the table are averages and standard deviations, respectively.

Table 2 also lists the absolute filter transmissivities derived by scaling of the calibration ratios to produce a transmissivity of 1 for filter number 0 (in fact, no filter).   Neutral density (base-10 logarithm of transmissivity) has also been computed and compared with its nominal value.   A small dependence on wavelength of the transmissivity of neutral-density filters was observed: The largest deviation from the values given in Table 2 was ~4%; the deviations in most of the samples remained within 1%. This small wavelength dependence has been neglected in the analysis.

4. Results

In this section the results of the aerosol optical depth measurement obtained at Lampedusa in the period from 28 June to 6 September 2000 are discussed. Only clear-sky cases were selected, because the same 74 mornings and afternoons that were used for calibration were examined and the same data were used. The general results are given here, with the purpose of demonstrating the ability of the technique to determine optical depth and highlight the evolution of short-term features.   We intend to present the diurnal evolution of the aerosol and other atmospheric parameters in relation to meteorological conditions and other possible causes in another paper.   Only measurements at 320.1 nm are displayed here, as the behavior of the data is similar to that at the other Brewer wavelengths.

Figure 3 shows the daily means of aerosol optical depth and the associated standard deviations.   The global average is 0.45 (with standard deviation 0.17), and values as low as 0.18 and as high as 0.77 were found; thus a large variability is present.   In the first part of the data set (until 12 August, i.e., Julian day 225) periods of high aerosol load ($\tau_{aer} > 0.6$) alternate with periods of low optical depth ($\tau_{aer} < 0.3$); the interval between maximum and minimum varies

from 3 to 6 days.   In the second part of the data set the aerosol shows a progressive increase, which lasts 2 weeks, at an average rate of 0.034 day^{-1} (from 0.20 on day 225 to 0.77 on day 242), followed by a decrease at an average rate of 0.044 day^{-1} (from 0.77 on day 242 to 0.46 on day 249).

As was pointed out above, the Langley plot calibration method requires a constant τ_{aer} for an entire morning or afternoon.   However, aerosols often present large variability, which can be observed not only as a day-to-day variation but sometimes on time scales as short as a few hours as well.   In these cases, the result of a Langley extrapolation can be expected to differ substantially from the correct extraterrestrial constant.   In Section 3 we eliminated such disturbances by using statistics and assuming that the variability behaves randomly; however, it is still of interest to review the data set and closely examine a few examples for illustration.

In Fig. 4 the daily evolution of τ_{aer} for 4 August 2000 (triangles) shows that the aerosol optical depth was low ($\tau_{aer} \simeq 0.2$) and remained almost constant during the morning (time <12 h).   This first part of the plot corresponds to the Langley plot in Fig. 1.
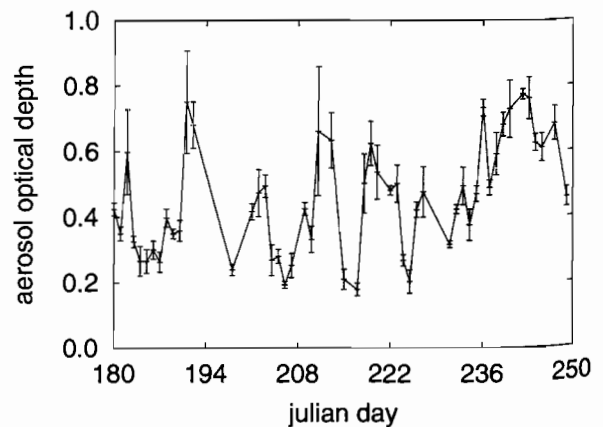

Fig. 3.   Mean daily values of aerosol optical depth (τ_{aer}) as derived by the Brewer spectrophotometer with ds measurements with all calibrated filters (0–3) at the 320.1-nm wavelength during the calibration campaign in year 2000.   The error bars display the statistical daily standard deviation, representative of the diurnal aerosol variability.
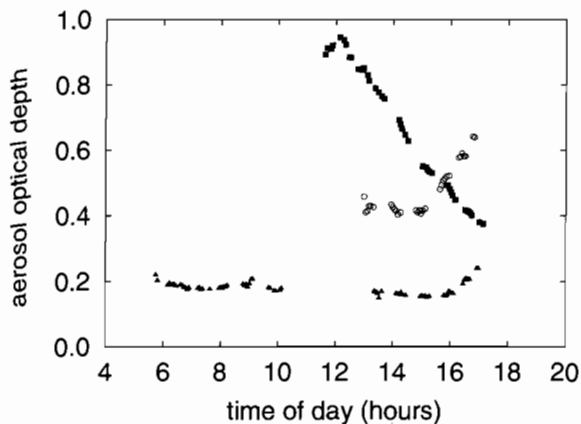
Fig. 4. Daily evolution of the 320.1-nm aerosol optical depth for three different days in summer 2000. Filled squares, 29 July; filled triangles, 4 August; open circles, 14 August.

For this case filter 3 calibration yields $I_0 = (4.122 \pm 0.034) \times 10^7$ photon counts at 320.1 nm, in agreement with the value given in Table 1, as expected because the optical depth remained constant during the morning. On the afternoon of the same day a small increase of τ_{aer} appears during the last hour of measurements. This variation is already large enough to alter substantially the value of I_0 that is obtained from the Langley plot: $(4.593 \pm 0.095) \times 10^7$ photon counts.

The behavior of τ_{aer} for 29 July (squares) and 14 August (circles) in Fig. 4 shows two extreme cases. On the afternoon of 29 July 2000 the aerosol decreased with time during the afternoon. Langley extrapolation yields $I_0 = (1.959 \pm 0.044) \times 10^7$, a value much smaller than the average. On 14 August 2000, τ_{aer} progressively increased with time, yielding a larger I_0 than expected: $(6.11 \pm 0.21) \times 10^7$.

The Langley extrapolation method would produce an incorrect estimate of the calibration constant if the aerosol optical depth varied with time. In fact, it is acknowledged that the statistical method used in Section 3 could be biased if a predominant daily evolution were present, e.g., with a maximum at noon. Thus it is extremely important to check carefully for the existence or absence of an aerosol daily evolution. Careful examination of all plots is necessary. In our case, the fact that the calibration constant taken from Table 1 coincides with that retrieved with constant aerosol conditions provides an indication that a bias, if present, is negligible.

Best Langley plots are obtained at high mountain sites, where a minimal influence from aerosols is expected. However, using the method illustrated above at a sea level station and taking all the necessary precautions to remove the effects of aerosol variations ensure the possibility to periodically check the calibration at the measurement site.

5. Validation

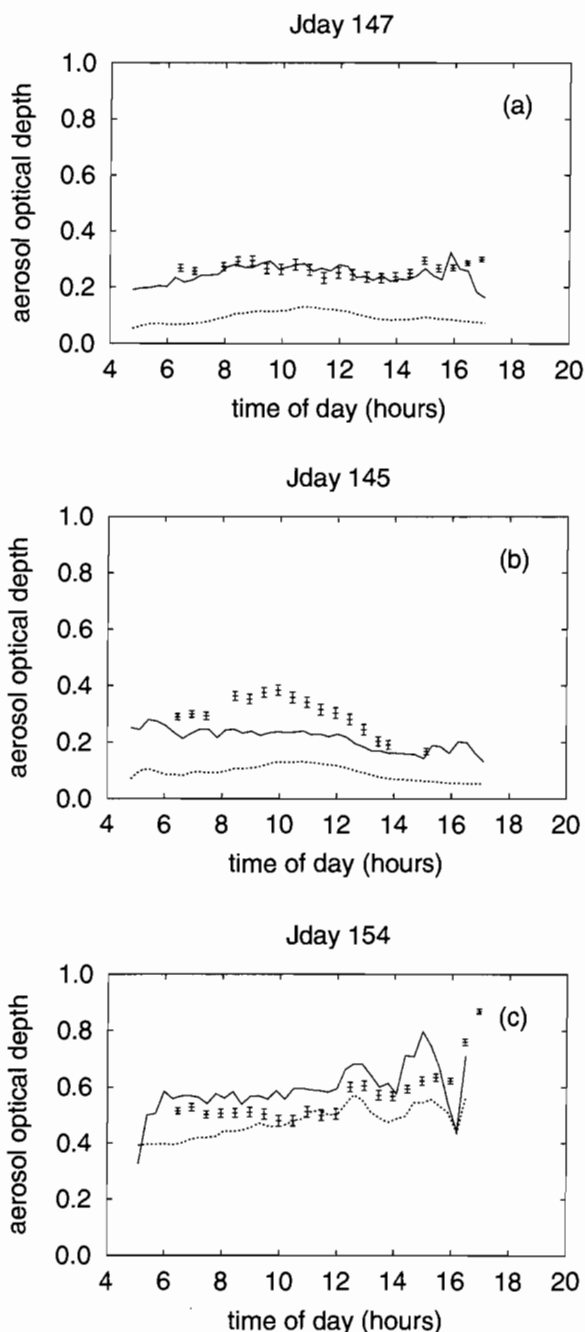Validation of the optical depths obtained with the method described above was achieved by their com-

Fig. 5. Aerosol optical depths for (a) 27 May 1999, (b) 25 May 1999, and (c) 3 June 1999: Comparison of measurements obtained with the Brewer spectrophotometer at 320.1 nm (points with error bars) and with the MFRSR at two wavelengths, 415 nm (solid curves) and 868 nm (dashed curves).

parison with independent measurements of the aerosol optical depth obtained with a multifilter rotating shadow-band radiometer (MFRSR). The MFRSR measured the global and diffuse components of solar irradiance at 415, 500, 615, 671, 868, and 937 nm, with a 10-nm effective bandwidth.[28]

During May and June 1999, the Photochemical Activity and Solar Ultraviolet Radiation Modulation Factors (PAUR-II) campaign took place in the Medi-
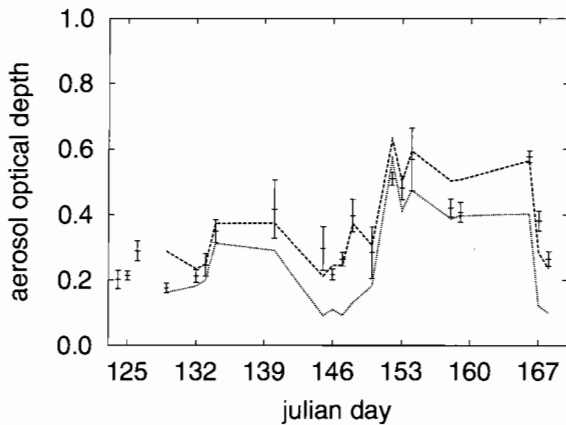
Fig. 6. Daily mean values of aerosol optical depth during the PAUR-II campaign held in 1999, as derived with the Brewer spectrophotometer at 320.1 nm (data points; the error bars display the daily standard deviation) and with the MFRSR at 415 nm (dashed curve) and 868 nm (dotted curve).

terranean.[29] The measurement sites were located on the islands of Crete and Lampedusa; the campaign was aimed at studying the effects of aerosols and ozone on ultraviolet irradiance. At Lampedusa, many instruments were operated simultaneously from 3 May to 18 June.[30] The campaign provided an opportunuty for the MFRSR and the Brewer spectrophotometer to perform simultaneous measurements. To validate our aerosol measurement method for the Brewer data we used the optical depths at 415 and 868 nm derived from the MFRSR measurements. The method for deriving the aerosol optical depth from the MFRSR measurements is described in Ref. 31.

Figure 5(a) depicts the measurements from the two instruments for 27 May 1999: The aerosol optical depths at 320.1 and 415 nm show good agreement, whereas much smaller values are measured at the longer wavelength. Close numerical agreement is not expected, as the measuring wavelengths differ by ~100 nm. The wavelength dependence of aerosols usually follows well a power law with a negative exponent, called the Ångström coefficient.[32] In previous studies carried out in a similar maritime environment it was found that the wavelength dependence seems to be steeper for low aerosol days and flatter on high aerosol days. Figures 5(b) and 5(c) seem to confirm these findings, although no general rule can actually be inferred from our data set.

In Fig. 5(b) a relatively small aerosol load is present, and its wavelength dependence is quite strong. In Fig. 5(c) we have a higher load and a weak wavelength dependence. It should be noted that short-time and small-amplitude features are often found in all the curves, though some unexplained discrepancies remain.

Figure 6 shows the overall evolution of the optical depth for the PAUR-II campaign at the three wavelengths. It can be seen that all measurements show a similar evolution, and on many days the optical
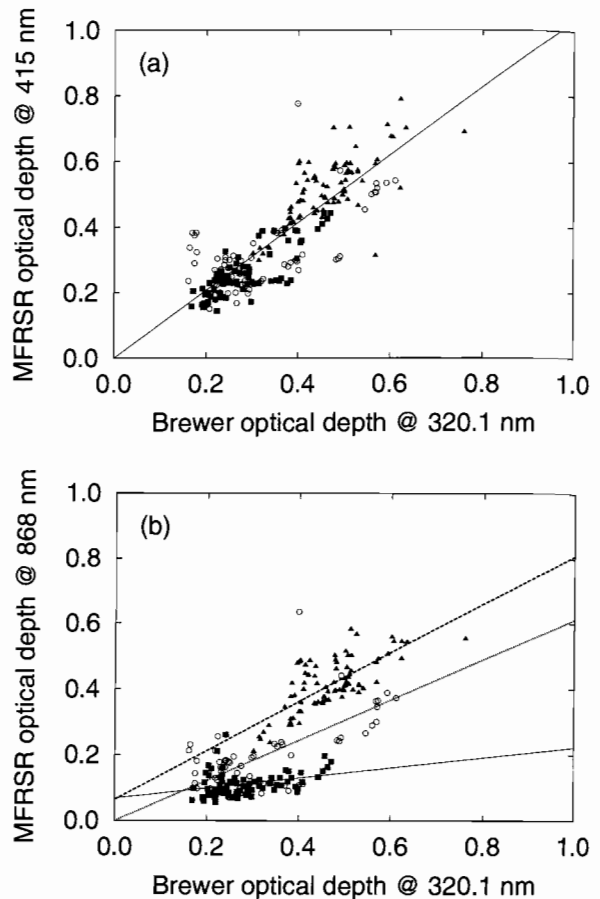

Fig. 7. Scatter plots of simultaneous optical depth measurements by Brewer at 320.1 nm and by MFRSR at (a) 415 nm and (b) 868 nm, obtained during the PAUR-II campaign held in 1999. The data points are organized into four classes (see text). Filled squares, class A points; open circles, class B and class C points; filled triangles, class D points. (a) Best-fit line of all data points together, (b) three different best-fit lines for class A data (solid line), classes B and C (dotted) and class D data (dashed line).

depths at 320.1 and 415 nm agree within the standard deviation. Figure 7(a) shows a scatter plot of the observations. This plot compares the Brewer measurements at 320.1 nm with the MFRSR data at 415 nm. A best-fit line ($y = a + bx$, with $a = 0.000 \pm 0.014$ and $b = 1.033 \pm 0.036$; correlation coefficient = 0.95) is also shown. Some scatter in the data set is present at these two wavelengths; however, there is reasonably good agreement.

The plot displayed in Fig. 7(b) was obtained at aerosol optical depths of 320.1 nm (from the Brewer spectrophotometer) and 868 nm (from the MFRSR). The data points appear much more widely separated than in Fig. 7(a). In both plots the data have been organized into classes according to the back trajectories of the various meteorological air masses, following Ref. 12. Class A (squares) includes all cases in which the trajectories do not pass over Africa, class B (circles) includes trajectories that marginally overpass Africa, class C (circles) comprises trajectories that spend only their last few days over Africa, and

Class	a	b	r
A	0.068 ± 0.011	0.155 ± 0.037	0.95
B + C	0.000 ± 0.030	0.612 ± 0.087	0.90
D	0.065 ± 0.025	0.745 ± 0.052	0.95

[a]For the $y = a + bx$ relationship, where x is the aerosol optical depth at 320.1 nm, and y is the aerosol optical depth at 868 nm; r is the correlation coefficient. The data were obtained during the PAUR-II campaign held at Lampedusa during 1999 and have been organized into classes A–D according to various meteorological conditions [see text and Fig. 7(b)].

class D (triangles) includes all trajectories that have spent a significant fraction of their past 10 days over the central Sahara. Thus, to a first approximation, class D represents the case in which desert aerosols coming from the Sahara are present, whereas class A contains few nondesert aerosols. Classes B and C, grouped together in Fig. 7, represent intermediate cases. For each class a different best-fit line has been drawn; thus the different wavelength dependences of the aerosols are shown. This is a signature of the different origin of the aerosols (different Ångström coefficients); see, e.g., Ref. 12. The line-fit parameters for Fig. 7(b) are listed in Table 3.

6. Calibration from Old Data

In Section 1 it was stated that our method is applicable without the need for any special measurement sequence; it requires only that the Brewer instrument be programmed to perform total ozone measurements. However, in Section 3 we introduced a special calibration sequence, obtained with a modification of the Brewer software (to force the filter selection) and a larger number of total ozone measurements than usual. The use of a special sequence, however, reduces the possibility of applying the method to old data or to data from stations where it is not possible to modify the instrumental software and schedule.

We want to show that the requirement of introducing a special measurement sequence can be relaxed, provided that the data include a consistent number of clean mornings and afternoons, each with a sufficient number of points so that these data may be used for Langley extrapolation. To do this we refer to the measurements from the PAUR-II campaign held in 1999, obtained before this research was begun, and

Table 4. Filter 3 Calibration Constants for Brewer Instrument # 123 Determined from the Data Set of the PAUR-II Campaign Held in 1999

Wavelength (nm)	I_0 for Filter 3 (photon counts $\times 10^7$)
303.2	2.592 ± 0.080
306.3	2.432 ± 0.068
310.1	2.060 ± 0.070
313.5	3.505 ± 0.104
316.8	3.729 ± 0.111
320.1	4.053 ± 0.116

investigate how they can be used for calibration. Only filter 3 data were considered, and 30 useful mornings and afternoons were selected. The number of data points available for each Langley plot is smaller than with the special calibration sequence described above (typically five or six, but in some cases as few as three), and air-mass factor values are confined to $1 < m < 2$. Therefore this data set would appear to be less than adequate for calibration purposes. We did, however, perform the calibration analysis described above on the PAUR-II data for illustration. The results are displayed in Table 4, which can be directly compared with Table 1. The 1999 calibration constants lie within 2σ from the year 2000 values, and for the four longest wavelengths they are within a 1σ limit. The standard deviations of the calibration constants displayed in Table 4 ($<4\%$) are only a little larger than the standard deviations shown in Table 1 ($\sim2\%$). It must also be noted that these results were obtained in a period characterized by large aerosol variability and unusually large values of τ_{aer} associated with desert dust events (see, e.g., Refs. 12 and 31).

7. Conclusions

The methodology described in this paper for the determination of aerosol optical depth from direct-sun measurements seems promising and can be applied simply to any of the Brewer instruments available around the world without the need for a complicated calibration apparatus.

Using the data from the total ozone measurement routine (ds) permits the use of a wide data set that is available from many stations. Moreover, we are convinced that Langley plot calibration can be used successfully when the necessary precautions are taken into account, even if it is performed at sea level. The method may be used for more-accurate climatological aerosol studies based on past and current Brewer data that are available at many stations in the worldwide Brewer network and without the need to change the instrumental setup and schedule.

For the Lampedusa station, Saharan dust is believed to be the major source of optical depth enhancement above the background level. Our analysis also shows the variegated wavelength dependencies of aerosol optical depth, which can be related to the aerosol type, and further confirms the use of multiwavelength measurements to characterize the air-mass type at each site. A smaller wavelength dependence is found for the high optical depth episodes associated with desert aerosols, suggesting the presence of larger particles than in the low-aerosol cases.

References

1. J. T. Houghton, L. G. Meira Filho, B. A. Callender, N. Harris, A. Kattenberg, and K. Maskell, eds., *Climate Change 1995:*

The Science of Climate Change (Cambridge U. Press, Cambridge, 1996).

2. I. N. Sokolik and O. B. Toon, "Direct radiative forcing by anthropogenic airborne mineral aerosols," Nature **381,** 681–683 (1996).

3. C. Morales, "The airborne transport of Saharan dust: a review," Clim. Change **9,** 219–241 (1986).

4. P. Chylek, G. B. Lesins, G. Videen, J. G. D. Wong, R. J. Pinnick, D. Ngo, and J. D. Klett, "Black carbon and absorption of solar radiation by clouds," J. Geophys. Res. **101,** 23,365–23,371 (1996).

5. I. Tegen, P. Hollrig, M. Chin, I. Fung, D. Jacob, and J. Penner, "Contribution of different aerosol species to the global aerosol extinction optical thickness: estimates from model results," J. Geophys. Res. **102,** 23,895–23,915 (1997).

6. R. J. Charlson, S. E. Schwartz, J. M. Hales, R. D. Cess, J. A. Coakley, Jr., J. E. Hansen, and D. J. Hofmann, "Climate forcing by anthropogenic aerosols," Science **255,** 423–430 (1992).

7. R. J. Charlson and M. J. Pilat, "Climate: the influence of aerosols," J. Appl. Meteorol. **8,** 1001–1002 (1969).

8. S. Twomey, "The influence of pollution on the shortwave albedo of clouds," J. Atmos. Sci. **34,** 1149–1152 (1977).

9. S. E. Schwartz and M. O. Andreae, "Uncertainty in climate change caused by aerosols," Science **272,** 1121–1122 (1996).

10. M. D. Loÿe-Pilot, J. M. Martin, and J. Morelli, "Influence of Saharan dust on the rain acidity and atmospheric input to the Mediterranean," Nature **321,** 427–428 (1986).

11. N. Kubilay and A. C. Saydam, "Trace elements in atmospheric particulates over the eastern Mediterranean: concentration, sources, and temporal variability," Atmos. Environ. **29,** 2289–2300 (1995).

12. A. di Sarra, T. Di Iorio, M. Cacciani, G. Fiocco, and D. Fuà, "Saharan dust profiles measured by lidar at Lampedusa," J. Geophys. Res. **106,** 10,335–10,347 (2001).

13. L. T. Molina and M. J. Molina, "Absolute cross-sections of ozone in the 185-to-350 nm wavelength range," J. Geophys. Res. **91,** 14,501–14,508 (1986).

14. J. B. Kerr, C. T. McElroy, D. I. Wardle, R. A. Olafson, and W. F. J. Evans, "The automated Brewer spectrophotometer," in *Atmospheric Ozone,* C. S. Zerefos and A. Ghazi, eds. (Reidel, Dordrecht, The Netherlands, 1985), pp. 396–401.

15. W. Josefsson, "Solar ultraviolet radiation in Sweden," in *SMHI Reports—Meteorology and Climatology* (Swedish Meteorological and Hydrological Institute, Stockholm, Sweden, 1986), vol. 53.

16. L. W. Thomason, B. M. Herman, and J. A. Reagan, "The effect of atmospheric attenuators with structured vertical distributions on air mass determinations and Langley plot analyses," J. Atmos. Sci. **40,** 1851–1854 (1983).

17. J. E. Hansen and L. D. Travis, "Light scattering in planetary atmospheres," Space Sci. Rev. **16,** 527–610 (1974).

18. P. M. Teillet, "Rayleigh optical depth comparisons from various sources," Appl. Opt. **29,** 1897–2000 (1990).

19. F. Marenco, V. Santacesaria, A. F. Bais, D. Balis, A. di Sarra, A. Papayannis, and C. Zerefos, "Optical properties of tropospheric aerosols determined by lidar and spectrophotometric measurements (Photochemical Activity and Solar Ultraviolet Radiation campaign)," Appl. Opt. **36,** 6875–6886 (1997).

20. A. F. Bais, C. S. Zerefos, and C. T. McElroy, "Solar UVB measurements with the double- and single-monochromator Brewer ozone spectrophotometer," Geophys. Res. Lett. **23,** 833–836 (1996).

21. A. F. Bais, "Absolute spectral measurements of the direct solar ultraviolet irradiance using a Brewer spectrophotometer," Appl. Opt. **36,** 5199–5204 (1997).

22. L. W. Thomason, B. M. Herman, R. M. Schotland, and J. A. Reagan, "Extraterrestrial solar flux measurements limitations due to a Beer's law assumption and uncertainty in local time," Appl. Opt. **21,** 1191–1195 (1982).

23. P. B. Russell, J. M. Livingston, E. G. Dutton, R. F. Pueschel, J. A. Reagan, T. E. Defoor, M. A. Box, D. Allen, P. Pilewskie, B. M. Herman, S. A. Kinne, and D. J. Hofmann, "Pinatubo and pre-Pinatubo optical-depth spectra: Mauna Loa measurements, comparisons, inferred particle size distributions, radiative effects, and relationships to lidar data," J. Geophys. Res. **98,** 22,969–22,985 (1993).

24. J. Jaroslawski and J. W. Krzyscin, "Aerosol optical depth in the UV range derived from direct sun ozone observations performed by the Brewer spectrophotometer Mark II No. 064 at Belsk, Poland," in *Atmospheric Ozone* (*Proceedings of the Quadrennial Ozone Symposium*) (Hokkaido U. Press, Sapporo, Japan, 2000).

25. A. W. Brewer, "A replacement for the Dobson spectrophotometer?" Pure Appl. Geophys. **106–108,** 919–927 (1973).

26. J. B. Kerr, C. T. McElroy, and R. A. Olafson, "Measurements of ozone with the Brewer ozone spectrophotometer," in *Proceedings of the Quadrennial Ozone Symposium, 4–13 August 1980* (International Ozone Commission, Boulder, Colo., 1980).

27. A. Bais, Department of Physics, Laboratory of Atmosphere Physics, Aristotle University of Thessaloniki, Thessaloniki, Greece (personal communication, 2001).

28. L. Harrison, J. Michalsky, and J. Berndt, "Automated multifilter rotating shadow-band radiometer: an instrument for optical depth and radiation measurements," Appl. Opt. **33,** 5118–5125 (1994).

29. C. S. Zerefos, "Photochemical activity and ultraviolet radiation modulation factors: an overview of the project," J. Geophys. Res., submitted for publication.

30. A. di Sarra, M. Cacciani, M. Campanelli, P. Chamard, C. Cornwall, J. De Luisi, L. De Silvestri, T. Di Iorio, P. Disterhoft, G. Fiocco, D. Fuà, P. Grigioni, W. Junkermann, F. Marenco, D. Meloni, F. Monteleone, and B. Olivieri, "Radiation, ozone, and aerosol measurements at Lampedusa during the PAUR-II campaign," in *IRS 2000: Current Problems in Atmospheric Radiation,* W. L. Smith and Yu. M. Timofegev, eds. (Deepak, Hampton, Va., 2001), pp. 1193–1196.

31. A. di Sarra, M. Cacciani, P. Chamard, C. Cornwall, J. De Luisi, T. Di Iorio, P. Disterhoft, G. Fiocco, D. Fuà, and F. Monteleone, "Effects of desert dust and ozone on the ultraviolet irradiance: observations at Lampedusa during PAUR-II," J. Geophys. Res. (to be published).

32. A. Ångström, "On the atmospheric transmission of sun radiation and on dust in the air," Georg. Ann. Deutch. **12,** 156 (1929), cited in E. Trakhovsky and E. P. Shettle, "Wavelength scaling of atmospheric aerosol scattering and extinction," Appl. Opt. **26,** 5148–5153 (1987).